One#Step Nucleic Acid Purification and Noise# Resistant Polymerase Chain Reaction by Electrokinetic Concentration for Ultralow#Abundance Nucleic Acid Detection

Author Manuscript

Title: One-Step Nucleic Acid Purification and Noise-Resistant Polymerase Chain Reaction by Electrokinetic Concentration for Ultralow-Abundance Nucleic Acid Detection

Authors: Wei Ouyang; Jongyoon Han

WILEY-VCH

One-Step Nucleic Acid Purification and Noise-Resistant Polymerase Chain Reaction by Electrokinetic Concentration for Ultralow-Abundance Nucleic Acid Detection

Wei Ouyang,[a] and Jongyoon Han*[a,b]

[a]   W. Ouyang and Prof. J. Han
        Department of Electrical Engineering and Computer Science and Research Laboratory of Electronics, Massachusetts Institute of Technology
        77 Massachusetts Avenue, Cambridge, MA, 02139, United States
        E-mail: jyhan@mit.edu
[b]   Prof. J. Han
        Department of Biological Engineering, Massachusetts Institute of Technology
        77 Massachusetts Avenue, Cambridge, MA, 02139, United States

        Supporting information for this article is given via a link at the end of the document.

Abstract: Nucleic acid amplification tests (NAATs) integrated on a chip hold great promises for early disease diagnosis at the point of care. Currently, nucleic acid (NA) purification remains complicated, time-consuming and labor-intensive, and it takes extensive efforts to optimize the amplification chemistry. Using selective electrokinetic concentration, we report one-step, liquid-phase NA purification that is much simpler and faster than conventional solid phase extraction. By further re-concentrating NAs and performing polymerase chain reaction (PCR) in a microfluidic chamber, our platform effectively suppresses non-specific amplification caused by non-optimal PCR designs. We achieved the detection of 5 copies of M. tuberculosis genomic DNA (equaling 0.3 cell) in real biofluids using both well-optimized and non-optimal PCR designs, which is 10× and 1000× fewer than those of the standard bench-top method, respectively. By significantly simplifying the workflow and shortening the development cycle of NAATs, our platform may find great uses in point-of-care diagnosis and beyond.

Introduction

Nucleic acid amplification tests (NAATs) play a crucial role in the analysis of low-abundance nucleic acids (NAs) for early diagnosis of diseases.[1–3] NAATs mainly rely on the gold-standard polymerase chain reaction (PCR),[4] though emerging isothermal amplification techniques like loop-mediated isothermal amplification (LAMP)[5] and recombinase polymerase amplification (RPA)[6] have attracted increasing interests.[2] Despite being highly powerful, NAATs generally suffer from the following major issues. (1) Lengthy design and optimization: Non-specific amplification is the most common problem that persists in NA amplification. A major source of non-specific amplification is the primer dimerization and subsequent elongation due to non-optimal primer design, reagent composition, and reaction conditions (*e.g.* temperature).[7–9] It often takes iterative optimizations to eliminate primer dimers, which is particularly challenging and lengthy for isothermal amplification techniques because of the low amplification temperatures that favor primer dimerization and the less established design methodologies.[2,10,11] (2) Complex workflows: Before amplification, NAs typically need to be extracted and stringently purified to remove amplification inhibitors (*e.g.* proteins and salts) from clinical samples, which is especially important for PCR. The mainstream technique for NA purification is the solid phase extraction (SPE), in which NAs are captured by silica membranes using chaotropic salts, washed with ethanol, and finally eluted from silica membranes (Figure 1A).[12–14] SPE is complex, time-consuming (typically 1-2 hours), labor-intensive, and relies on equipment and amplification-inhibitive chemicals. Moreover, SPE has limited recovery efficiency and is susceptible

to cross-contamination, which limits the sensitivity and specificity of detection. Solid phase microextraction (SPME) is a relatively new NA purification technique, in which NAs are extracted by a sorbent-coated fiber followed by a desorption step in NaCl solution.[15,16] Compared to SPE, SPME has reduced steps and avoids the use of centrifugation and PCR-inhibitive chemicals. However, the NA extraction efficiency of SPME is much lower than that of SPE, and it still requires a vortex mixer to enhance NA adsorption, takes about 45 min, and has a sample carryover problem.[15–17]

Fully integrated NAATs on microfluidic chips with sample-to-answer capability have attracted significant interests in recent years, which can potentially be implemented at the point of care without the need for trained personnel and centralized labs.[4,18–23] However, existing works toward fully integrated NAATs still have several major limitations. First, the amplification chemistry for integrated NAATs is typically obtained following the design and optimization processes for bench-top NAATs, which is too lengthy and sophisticated for emergency situations (*e.g.* outbreaks of new pathogens) and point-of-care applications. Second, on-chip NA purification still relies on the SPE following the bind-wash-elute procedure (in a miniaturized format), which requires complicated fluidic/valving structures and complex operation protocols.[12,24–27] The dependence on miniaturized SPE makes NAATs difficult to automate, time-consuming, and less robust. Third, the miniaturization of NAATs on microfluidic chips is often accompanied by the significant decrease of sample processing throughput (<10 µL),[4] which disallows the capture of sufficient copies of ultralow-abundance NAs (<1 copy/µL)[28] for subsequent detection, thereby fundamentally limiting the detection sensitivity. Taken together, in order to detect ultralow-abundance NAs rapidly and reliably, it is important to develop integrated NAATs with short design cycles, simple NA purification methods, and high sample processing throughputs.

In recent years, isotachophoresis (ITP) on microfluidic chips has emerged as a non-solid-phase, one-step NA purification technique that takes only minutes, which greatly simplifies the workflow of NA purification.[29] ITP utilizes the electrophoretic stacking and separation of NAs from other species in the presence of a leading electrolyte (LE) and a tailing electrolyte (TE), whose separation performance and extraction efficiency are critically dependent on the ion species, ion mobility, ion concentration, volume, pH, and temperature of the TE/LE.[30] This strong dependence not only requires fine tuning of the chemistry for different samples, but also poses challenges for high-throughput processing as the chemical environment degrades (*e.g.* pH shift) with electrochemical reactions.[30] The pioneering works of Santiago *et al.* focused on ITP-based NA purification for off-chip amplifications, with a maximum

throughput of 25 µL reported.[31–38] The commercial product of ITP-based NA purification, Ionic Purification System (Purigen Biosystems, Pleasanton, CA), can process up to 200 µL samples per run but yields an elution volume of 40 µL, which is not suitable for microfluidic applications. Posner *et al.* combined ITP and LAMP/RPA to develop fully integrated microfluidic NAATs with NA extraction efficiency of ~10% in milk and sample throughputs of 15-20 µL, achieving detection limits of ~10 copies/µL (~16 aM).[39,40] To detect ultralow-abundance NAs (<1 copy/µL), the sample processing throughputs and/or NA extraction efficiency of ITP-based NAATs remain to be improved. Lastly, existing works on ITP-based NAATs did not address the aforementioned issue of long design cycles of amplification chemistry.

Here we report an integrated NAAT using hierarchical selective electrokinetic concentration with three key features: one-step NA purification, high sample processing throughputs, and PCR resistant to non-specific amplification ("noise-resistant") even with non-optimal designs. First, we realize one-step NA purification using selective electrokinetic (EK) concentration. In an EK concentration device, biomolecules are electroosmotically injected into a microfluidic channel and subsequently trapped by the locally amplified electric field in the ion depletion zone induced by an ion-selective membrane, leading to the continuous stacking/concentration of biomolecules.[41–46] More recently, we demonstrated selective EK concentration by superposing an appropriate pressure-driven flow with electroosmosis, which enabled proteins (low electrophoretic mobility) to escape the ion depletion zone yet still kept NAs (high electrophoretic mobility) trapped, thereby selectively concentrating NAs.[47] In this work, we propose that selective EK concentration can be used as "EK purification" to purify NAs and effectively remove unwanted biochemical species for subsequent PCR. The behavior of NAs in selective EK concentration is determined by their electrophoretic mobility,[42,45–47] and their electrophoretic mobility is sequence-independent and constant for NAs above ~100 bp (decreasing by <= 10% below 100 bp).[48] Therefore, EK purification can potentially be seamless used for NAs of various sequences, sizes, and origins. Compared to the conventional bind-wash-elute approach, EK purification is a liquid-phase, physical method performed in one step by simply applying a DC voltage and a hydrostatic pressure, eliminating the needs for complex device design, multi-step operations, and PCR-inhibitive chemicals. Compared to ITP, EK concentration does not require leading/tailing electrolytes and works in a wide range of buffer compositions, buffer concentrations, pHs, and other conditions,[49] making it easily adaptable to different samples. Second, we recently achieved high sample processing throughputs by massive parallelization of electrokinetic concentrators, which could process 0.1-10 mL samples in 15 min depending on the number of parallel concentrators.[50] In this work, as a proof of concept, we demonstrate an integrated NAAT with a throughput of 150 µL in 15 min by using 64 parallel concentrators, which enables the detection of ultralow-abundance NAs (<1 copy/µL) in our platform. Third, we use a hierarchical electrokinetic concentration architecture to re-concentrate purified NAs from massively parallel concentrators into a single concentrator, which are subsequently delivered into a microfluidic chamber for PCR. By concentrating NAs and performing PCR in a microfluidic chamber with a small volume of reagents (~0.1 µL), we keep the same number of the target template but dramatically decrease the number of primer dimers compared to that in conventional tube-based PCR (~20 µL), thereby greatly enhancing the signal-to-noise ratio. Also, increasing the concentration of the target template will exhaust the reagents at earlier cycles, thereby suppressing the amplification of primer dimers that typically occur at large cycle numbers. In sum, by combining hierarchical selective EK concentration and microfluidic PCR (HSEC-PCR) as shown in Figure 1B, we can create an integrated NAAT platform with one-step NA purification and noise-resistant PCR for the rapid and reliable detection of ultralow-abundance NAs.

The diagnosis of *M. tuberculosis* (MTB) from urine and blood-derived samples has attracted a lot of interests recently,[51] because these samples are easily accessible from any age groups and can be used for the detection of both pulmonary and extrapulmonary TB. In recent studies,[52,53] qPCR-based amplification of MTB-specific DNAs purified from equivalently 50-500 μ L urine and plasma show quantification cycle (C_q) values as low as ~40 (corresponding to nearly a single target DNA copy), indicating target DNA concentrations as low as ~0.01 aM. By spiking MTB genomic DNAs in real biofluids, we demonstrate that HSEC-PCR achieved the detection of 0.05 aM target DNA from 150 µL urine and 0.2 aM from 37.5 µL serum. The standard method using bench-top SPE and PCR achieved the detection of similar concentrations of 0.04 aM MTB genomic DNA from 2 mL urine and 0.4 aM from 200 µL serum but with a more complex workflow and longer time. The corresponding lowest detectable DNA copy numbers were 5 copies for HSEC-PCR and 50 copies for bench-top SPE and PCR, because of the higher recovery efficiency of HSEC-PCR than the standard method. In the case of non-optimal PCR designs, we demonstrate that HSEC-PCR retained the same detection limit by suppression of non-specific amplification, which is two orders of magnitude enhancement compared to that of the standard method in terms of DNA concentration and three orders of magnitude in terms of DNA copy number. This platform solves the universal limitations of NAATs, which can be directly used for isothermal amplifications and other amplification techniques.

Results and Discussion

Figure 1C and Figure 1D show the schematic and photo of the HSEC-PCR device, respectively. The device consists of two stages. In the first stage, there are 64 parallel microchannels (200 µm wide) and 1 buffer channel (200 µm wide) on each side, all of which are 13 µm deep. A cation-selective Nafion membrane strip (~1 µm thick) patterned on the glass slide crosses the microchannels perpendicularly at the bottom of the microchannels, which is used to generate the EK concentration effect under an appropriate DC voltage configuration. The right end of the first stage has 1 microchannel in the middle connecting to the second stage and 2 outlets. The second stage consists of 1 microchannel of 800 µm wide and 13 µm deep, 1 PCR chamber of 1 mm long, 1 mm wide, and 80 µm deep, and 1 Nafion membrane strip for the generation of the EK concentration effect. Having a deep PCR chamber is important for reducing the water evaporation through the highly permeable PDMS, owing to the lower surface-area-to-volume ratio than a shallow PCR chamber.[54] Four pneumatic valves are used for the manipulation (isolation, transfer, and mixing) of the concentrated NAs. Figure 1E shows the device placed on the MiniPCR[TM] thermal cycler (Amplyus, Cambridge, MA) during qPCR. Figures 1F-1H show the bright-field micrographs of the first stage, intersection between the first and second stages, and the second stage, respectively. Supporting pillar arrays are used to prevent the collapsing of the microfluidic channels. Device fabrication is described in Supporting Information.
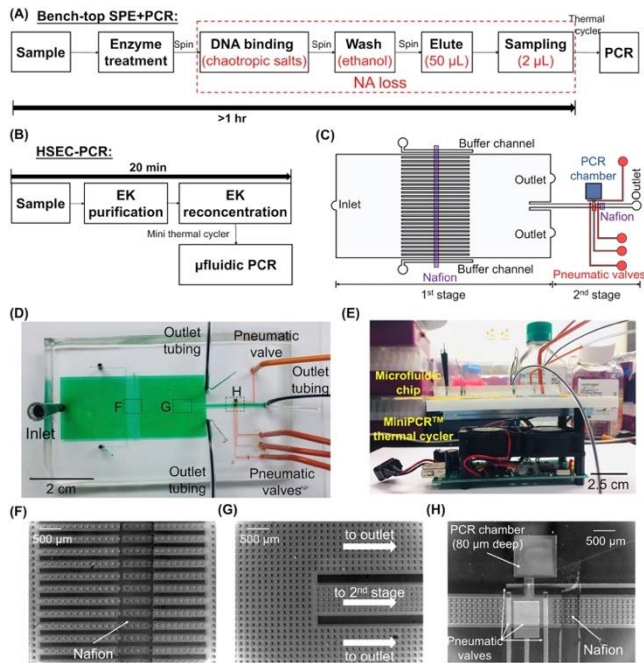
2

Figure 1. Schematic and photos of the HSEC-PCR device. (A) Workflow of the standard bench-top SPE+PCR, which requires multiple steps and typically takes more than an hour to purify NAs. (B) Workflow of HSEC-PCR, which uses one-step NA purification followed by reconcentration of purified NAs for PCR (20 min, not including the time of PCR). (C) Schematic of the HSEC-PCR device. (D) Photo of the HSEC-PCR device. (E) Photo of the device placed on the MiniPCR™ thermal cycler. (F) Micrograph of the first stage. (G) Micrograph of the intersection between the first and second stages. (H) Micrograph of the second stage.

Figure 2 shows the principle and operation procedures of HSEC-PCR. In EK purification, the inlet is set to a positive voltage *V*, and the outlets and side buffer channels are grounded. A hydrostatic pressure *P* is applied by the control of the liquid level difference between the inlet and outlet tubings.[47] The principle of EK purification is explained as follows. Under the aforementioned electrical configuration, the electric potential difference between the parallel microchannels and the side buffer channels induces selective transport of cations through Nafion from the parallel microchannels to the side buffer channels, leading to the generation of ion depletion zones in the parallel microchannels near Nafion (to the left side). The electric field is significantly amplified in the ion depletion zone, which functions as an electric force barrier (Figure 2A). The biomolecules (mainly NAs and proteins) enter the microchannels with the fluid flow induced by electroosmosis (EO) and pressure-driven flow (PDF),[55] which has a velocity of $v_{EO} + v_{PDF}$ (rightward). At the same time, biomolecules are subject to an electrophoretic force that generates an electrophoresis (EP) velocity of $v_{EP} = \mu \cdot E$ (leftward), where μ is the electrophoretic mobility of the biomolecules and *E* is the amplitude of electric field. The biomolecules continuously enter the microchannels because $v_{EO} + v_{PDF} > v_{EP}$ in the bulk of the microchannels. As the biomolecules enter the ion depletion zones with the amplified electric field, v_{EP} gradually increases with *E* until it becomes as great as $v_{EO} + v_{PDF}$ (i.e. $v_{EO} + v_{PDF} = v_{EP}$), leading to the electrokinetic trapping and continuous stacking of the biomolecules, i.e. the EK concentration effect. However, if the maximum v_{EP} in the ion depletion zones (at the peak of the electric force barrier E_{max}) is still less than $v_{EO} + v_{PDF}$, i.e. $v_{EO} + v_{PDF} > v_{EP\_max} = \mu \cdot E_{max}$, the biomolecules will overcome

the electric force barrier and not be concentrated. Given that the electrophoretic mobility of NAs is much greater than that of proteins (and other unwanted biochemical species) ($\mu_{NA} \gg \mu_{protein}$),[29,56] it can be satisfied that $v_{EP\_max}(NA) > v_{EO} + v_{PDF} > v_{EP\_max}(protein)$ by appropriate modulation of the pressure-driven flow (v_{PDF}), thereby only concentrating NAs and simultaneously removing proteins. We optimized the conditions of EK purification by using human urine spiked with 100 nM Alexa Fluor 647-labeled DNA as the sample. The native fluorescence of proteins and metabolites in urine can be imaged using the green fluorescence setup (excitation wavelength ~490 nm) at a long exposure time of 1000 ms. A voltage of 250 V was applied to the device. As shown in Figure 2A (right), both the DNA (shown in green) and proteins and metabolites (shown in red) were concentrated under a zero hydrostatic pressure; however, only the DNA was concentrated and the proteins and metabolites were removed under a hydrostatic pressure of 400 Pa, which was the condition used for subsequent experiments.

As shown in Figure 2B, after EK purification, the outlets of the first stage are closed, and that of the second stage is opened and grounded. The conditions of the inlet remain *V*=250 V and *P*=400 Pa. Under this configuration, the NAs concentrated in the parallel microchannels in the first stage are flushed toward the second stage, and re-concentrated near the Nafion in the second stage. Finally, the re-concentrated NAs are isolated by the pneumatic valves and transferred into the PCR chamber (pre-loaded with PCR reagents) for amplification.
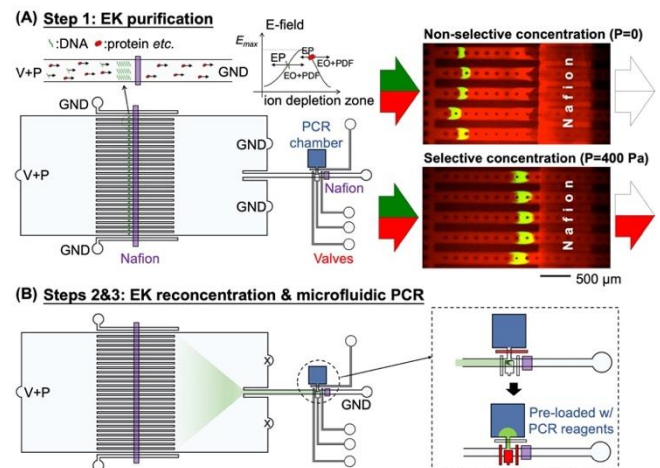

Figure 2. Principle and operation procedures of HSEC-PCR. (a) EK purification of NAs in the first stage, with a DC voltage and a hydrostatic pressure applied to the inlet and the two outlets of the first stage grounded. In the non-selective concentration mode (*P*=0), both the DNA (green fluorescence) and proteins and metabolites (red fluorescence) were concentrated; In the selective concentration mode (*P*>0), only the DNA was concentrated while the proteins and metabolites went downstream and were removed from the device. (b) EK re-concentration of NAs near the Nafion membrane in the second stage by closing the outlets of the first stage and opening that of the second stage, followed by transfer of NAs into the PCR chamber (pre-loaded with PCR reagents) for amplification through controlling the pneumatic valves.

We next visualized the whole workflow of HSEC-PCR using MTB genomic DNA (target sequence concentration: 5 copies/µL), 10 mg/ml BSA, and 100 nM fluorescently labeled DNA spiked in human urine. As shown in Figure 3 (left images), the DNAs were first selectively concentrated in the 64 parallel microchannels in the first stage. A volume of ~150 µL was processed in 15 min. Next, the device was reconfigured as previously mentioned to transfer the concentrated DNAs into the second stage (Figure 3,

3

middle). The DNAs were re-concentrated in the second stage within 3 min. The re-concentrated DNAs were then isolated in the microchannel by closing a pair of pneumatic valves (Figure 3, right). Next, the valve for the PCR chamber was opened, and the large-area valve was used as a mixer to drive the fluid and DNAs into the PCR chamber. As shown in Figure 3, after 15 on-and-off cycles, the majority of the DNAs entered the PCR chamber. Finally, the valve for the PCR chamber was closed, followed by qPCR through thermal cycling. The fluorescence intensity (using green fluorescence setup) of the PCR chamber increased as qPCR proceeded. Note that, although the genomic DNA was not fully mixed in the PCR chamber initially, the short DNA amplicons mixed thoroughly by diffusion within the first few PCR cycles (diffusion time is ~15 min according to a previous study[54]). To characterize the DNA extraction efficiency, we spiked 1 nM fluorescently labeled DNA in 150 µL urine/0.25×serum (a total of 150 fmol) and measured the fluorescence intensity of DNAs extracted into the PCR chamber. We also measured the fluorescence intensity of 150 fmol DNAs directly spiked into the PCR chamber. As described in detail in Section 5 of Supporting Information, the extraction efficiency is the ratio of the fluorescence intensities of extracted DNAs to that of the total spiked DNAs, which were 84.4% for urine and 74.6% for serum.
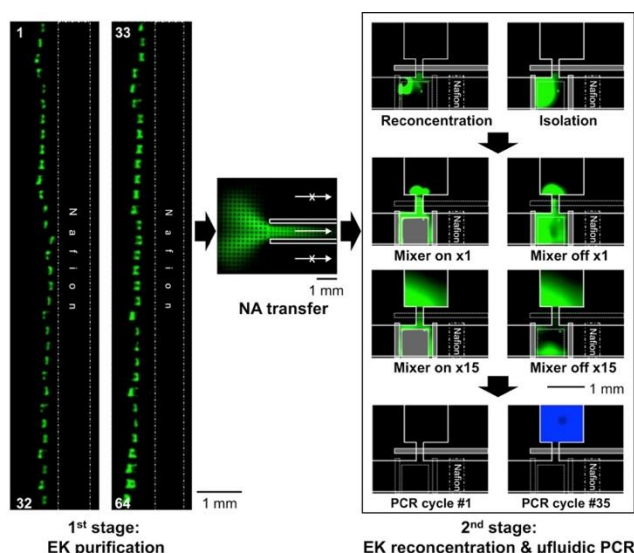

Figure 3. The workflow of HSEC-PCR visualized by fluorescently labeled DNA. The left images showed the EK-concentrated DNAs in the parallel microchannels in the first stage during EK purification. The middle image is at the intersection of the first and second stages, which shows the transfer of the concentrated DNAs from the first stage to the second stage. In the right images, the re-concentrated DNAs were isolated by a pair of pneumatic valves and transferred into the PCR chamber by the cyclic on-and-offs of a large-area pneumatic valve that served as a mixer. Finally, qPCR was performed in the PCR chamber, the fluorescence of which increased as qPCR proceeded.

We compared the performance of HSEC-PCR with that of the standard bench-top SPE+PCR method by amplifying a highly specific sequence in the IS6110 region of the MTB genome (16 copies per genome) using a well-optimized probe-based qPCR (primer set A and probe A, Table 1, see Supporting Information for details).[57] First, we established the benchmark using standard bench-top SPE+PCR with the leading NA purification kits on the market by following the procedures outlined in Figure 1A. The Norgen Urine DNA Isolation Kit could process 2 mL urine per spin column, and the Qiagen QIAamp

DNA Blood Mini Kit could process 0.2 mL serum per spin column. By 10× serial dilution with human urine starting from stock MTB genome extract (ATCC, Manassas, VA, see Supporting Information for details), we prepared samples with 3×10^4, 3×10^3, 3×10^2, 3×10^1, 3, 0.3, and 0 copies of the MTB genome (corresponding to 5×10^5, 5×10^4, 5×10^3, 5×10^2, 5×10^1, 5, and 0 copies of the target DNA) in 2 mL human urine, yielding target DNA concentrations of 400, 40, 4, 0.4, 0.04, 0.004, and 0 aM. We then purified the spiked human urine samples with the Norgen Urine DNA Isolation Kit, which took 100 min. Similarly by serial dilution, we prepared samples with 3×10^4, 3×10^3, 3×10^2, 3×10^1, 3, 0.3, and 0 copies of the MTB genome (corresponding to 5×10^5, 5×10^4, 5×10^3, 5×10^2, 5×10^1, 5, and 0 copies of the target DNA) in 0.2 mL human serum, yielding target DNA concentrations of 4000, 400, 40, 4, 0.4, 0.04, and 0 aM. We then purified the spiked human serum samples with the Qiagen QIAamp DNA Blood Mini Kit, which took 65 min. Figure 4A and Figure 4B show the amplification curves of the purified DNAs at different total spiked copy numbers in urine and serum using a bench-top thermal cycler, respectively. The target DNA was detectable when the total spiked copy number of the target DNA was as low as 50 copies, both for urine and serum. The main factor limiting the detection of lower copy numbers is that, as a conventional practice, only a small fraction of the eluate (2 µL in this work) from the total 50 µL eluate (1/25) could be used for PCR, because of the high cost and slow thermal conduction of large-volume PCR.[58] The corresponding C_q values of the qPCR were compared in Figure 4C. The C_q values were very similar for the same total spiked DNA copy numbers in urine and serum, though the concentrations were different by one order of magnitude. This observation indicates that the recovery of the DNA purification kits is largely independent of the DNA concentration. The efficiencies of PCR for DNAs purified from urine and serum were both ~95% (calculated from the slopes of the fitted lines), indicating good removal of PCR inhibitors by the purification kits.

We next used HSEC-PCR for integrated purification, amplification, and detection of the target DNA. As previously mentioned, the device was able to process 150 µL samples in 15 min. Similarly by serial dilution, we prepared samples with 3×10^2, 3×10^1, 3, 0.3, and 0 copies of the MTB genome (corresponding to 5×10^3, 5×10^2, 5×10^1, 5, and 0 copies of the target DNA) in 150 µL human urine, yielding target DNA concentrations of 55, 5.5, 0.5, 0.05, and 0 aM. Also by serial dilution, we prepared samples with 3×10^2, 3×10^1, 3, 0.3, and 0 copies of the MTB genome (corresponding to 5×10^3, 5×10^2, 5×10^1, 5, and 0 copies of the target DNA) in 37.5 µL human serum, yielding target DNA concentrations of 220, 22, 2.2, 0.2, and 0 aM. The spiked serum samples were diluted to 150 µL with 1×PBS, which was necessary for stable EK concentration of the DNAs.[50] As shown in Section 6 of the Supporting Information where we performed microfluidic PCR directly with NAs in urine/serum backgrounds without HSEC, PCR was strongly inhibited by the PCR inhibitors in urine/serum. As shown in Figure 4D and Figure 4E, HSEC-PCR could detect as low as 5 copies of the target DNA in both urine and serum, indicating the good removal of PCR inhibitors and good recovery of the DNAs by HSEC. At very low copy numbers (50 and 5), the variances between the C_q values of different runs were significantly greater than those of higher copy numbers. This can be attributed to the incomplete collection of NAs into the PCR chamber during the purification, re-concentration, isolation and mixing process, which generates more significant variances at very low copy numbers statistically. Although HSEC-PCR achieved the detection of lower copy numbers (5 v.s. 50) than standard SPE+PCR, the corresponding lowest detectable DNA concentrations were similar (0.05 v.s. 0.04 aM in urine and 0.2 v.s. 0.4 aM in serum), because the current HSEC-PCR device had lower throughputs than the SPE spin columns did (0.15 v.s. 2 mL for urine and 37.5 µL v.s. 200 µL for serum). In the future,

4

we can increase the number of parallel microchannels in the first stage of the device to increase the throughput (up to 10 mL) and hence potentially detect much lower concentrations, as we have demonstrated elsewhere.[50] Finally, as shown in Figure 4F, the efficiencies of HSEC-PCR were 87.1% and 79.1% for urine and serum, respectively, which were lower than those of standard bench-top SPE+PCR. This is commonly observed in microfluidic PCR systems, which can be attributed to a number of reasons, such as non-optimal thermal cycling conditions and the adsorption of polymerase on the PDMS surfaces of the PCR chamber.[59,60]

Table 1. Sequences of qPCR primers and probe. In Probe A, 6-FAM is the fluorescence dye at 5' and ZEN[TM] and IABkFQ[TM] (Iowa Black FQ) are the double fluorescence quenchers (Integrated DNA Technologies, IA).

Name	Sequence (5'→ 3')
Forward primer A	CGA TGT GTA CTG AGA TCC CCT ATC CG
Reverse primer A	GGC CTT TGT CAC CGA CGC C
Probe A	/56-FAM/ AAC GTC TTT /ZEN/ CAG GTC GAG TAC GCC TT /3IABkFQ/
Forward primer B	ACC AGC ACC TAA CCG GCT GTG G
Reverse primer B	CAT CGT GGA AGC GAC CCG CCA G

We next tested the SYBR Green-based qPCR with primer set B (as listed in Table 1, see Supporting Information for details)[61] using the standard bench-top SPE+PCR and analyzed the PCR products using gel electrophoresis (blueGel[TM], Amplyus, Cambridge, MA). SYBR Green is a commonly used intercalating dye for the real-time quantification of PCR by binding non-specifically to double-stranded DNA, which avoids the use of expensive qPCR probes. As shown in Figure 5A, only a band of the 130-bp amplicon was observed from the PCR product of the target DNA (10^5 spiked copies) purified from 2 mL human urine. However, in the no-template control with only DI water, multiple bands of non-amplicons were observed, indicating non-specific amplification due to primer dimers. The gel electrophoresis result clearly indicates that PCR is a competition for reagents between specific and non-specific amplifications: the specific amplification strongly suppressed non-specific amplification in the presence of high-abundance target DNA, while the non-specifically amplified products prevail in the presence of low-abundance target DNA. As shown in Figure 5B, in standard bench-to SPE+PCR, 500 or fewer copies of the target DNA could not be distinguished from 0 copy of the target DNA due to strong non-specific amplification, indicating a lowest detectable copy number of 5000 (corresponding to 4 aM). A PCR efficiency of 107.88% (Figure 5C) in bench-top PCR indicates that DNAs were generated faster than a standard 2-fold replication per cycle (100%), which was caused by the additional fluorescence signal from non-specific amplification (especially at low target DNA concentrations). In HSEC-PCR, the target DNA molecules were concentrated into a microfluidic chamber (~0.1 μL), in which there were much fewer primer dimers than a conventional tube (~20 μL). With the all the DNAs collected into the microfluidic chamber but with much fewer primer dimers, the signal-to-noise ratio is greatly enhanced, thereby enabling the detection of lower copy numbers of the target DNA. Also, increasing the concentration of the target DNA will exhaust the reagents at earlier cycles, thereby suppressing the amplification of primer dimers that typically occur at large cycle numbers. As shown in Figure 5D, although non-specific amplification was still observed in HSEC-PCR using primer set B, as low as 5 copies of the target DNA was distinguishable from 0 copy of the target DNA, indicating the effective suppression of non-specific amplification. HSEC-PCR was able to detect 5 copies of the target DNA (corresponding to 0.05 aM) even using a non-optimal PCR design, which is three orders of magnitude better than that achieved by the standard bench-top PCR in terms of copy number and two orders of magnitude better in terms of concentration. A PCR efficiency of 74.6% was achieved by HSEC-PCR (Figure 5E), which was attributed to similar factors discussed previously. This result suggests that HSEC-PCR can significantly shorten the development cycle of NAATs by skipping the lengthy optimization process for primer dimer elimination and still achieving good detection sensitivity with non-optimal PCR designs.
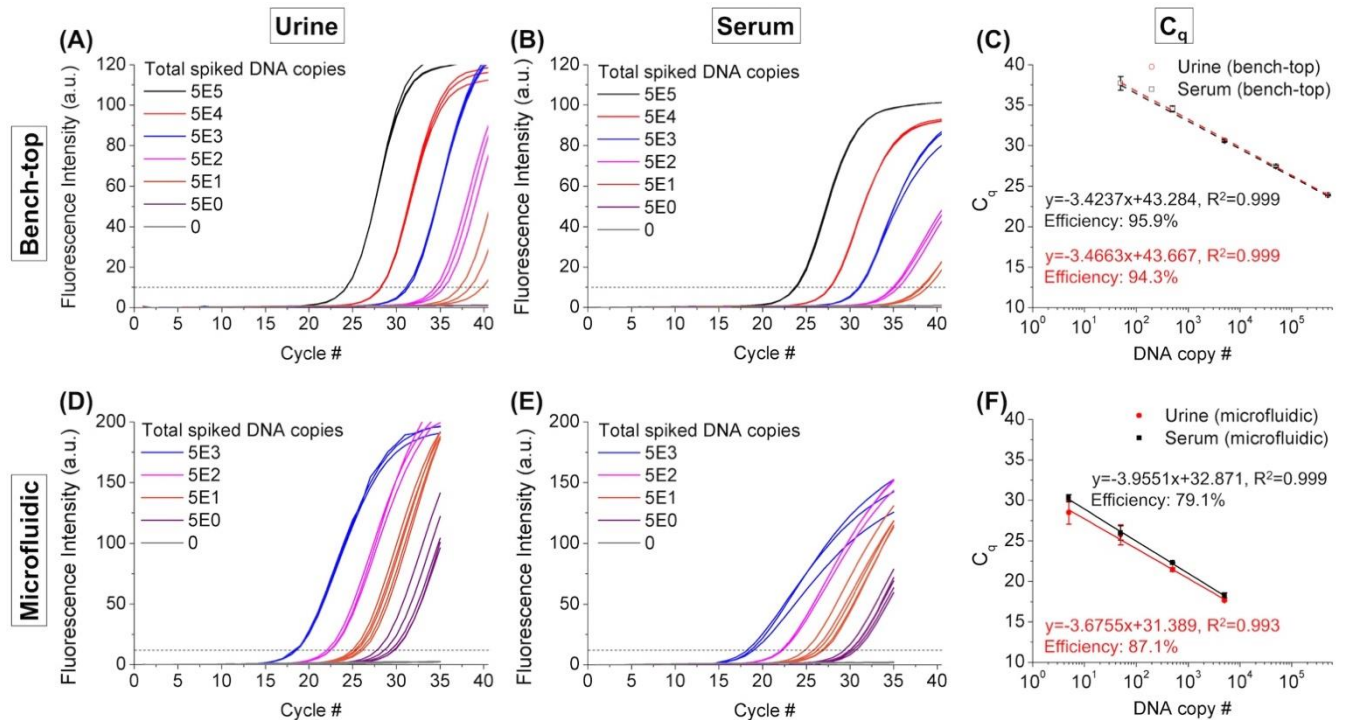
5

Figure 4. Performance of standard bench-top SPE+PCR and HSEC-PCR for detecting DNA spiked in human urine and serum using probe-based qPCR (primer set A and probe A). Amplification curves of the target DNA purified from (a) urine and (b) serum, and (c) the corresponding C_q values for different total spiked DNA copy numbers using standard bench-top SPE+PCR, indicating a lowest detectable amount of 50 copies. Amplification curves of the target DNA purified from (d) urine and (e) serum, and (f) the corresponding C_q values for different total spiked DNA copy numbers using HSEC-PCR, indicating a lowest detectable amount of 5 copies.
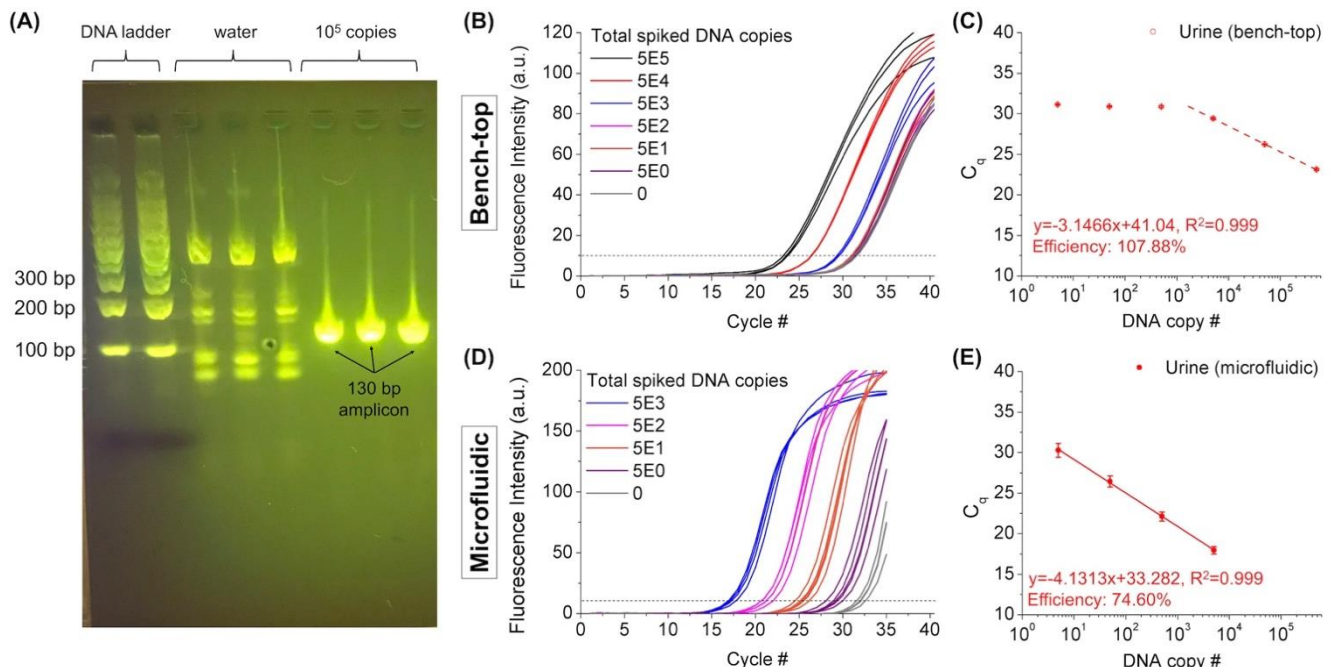

Figure 5. Performance of standard bench-top SPE+PCR and HSEC-PCR for detecting DNA spiked in human urine using a non-optimal PCR design (primer set B). (A) Gel electrophoresis result of PCR products using standard bench-top SPE+PCR. The non-specific amplification products from DI water indicates the formation of primer dimers and their elongation during amplification. (B) Amplification curves for different total spiked DNA copy numbers using standard bench-top SPE+PCR. The lowest detectable amount of the target DNA was 5000 copies, because the strong non-specific amplification from primer dimers masked the signals from lower amounts of the target DNA. (C) C_q values for different total spiked DNA copy numbers using standard bench-top SPE+PCR. (D) Amplification curves for different total spiked DNA copy numbers using HSEC-PCR. As low as 5 copies was detectable even with non-optimal primers, because the suppression of non-specific amplification in HSEC-PCR. (E) C_q values for different total spiked DNA copy numbers using HSEC-PCR.

6

Conclusion

In this paper, we have demonstrated HSEC-PCR as an integrated platform with one-step NA purification and noise-resistant quantitative PCR for rapid and reliable detection of ultralow-abundance NAs in real biofluids. Compared to conventional SPE-based NA purification methods (bench-top or microfluidic format), EK purification is a one-step, liquid-phase, non-binding approach with the advantages of short processing time (20 min), low cost, simple device design and operation protocols, and avoiding the use of PCR-inhibitive chemicals. Unlike standard bench-top PCR, HSEC-PCR is resistant to non-specific amplification caused by primer dimers in non-optimal PCR designs and retains a very low detection limit (0.05 aM, 5 DNA copies in 150 μ L), thereby greatly shortening the development cycle of NAATs. Some of the future work of this platform includes: (1) Further increase of the sample processing throughput by higher parallelization to enable the detection of even lower abundance NAs. (2) Demonstrating the versatility of this platform in detecting NAs of various sources (*e.g.* mammalian, plant, bacterial, viral DNAs and RNAs of different sizes) from various specimens (blood, plasma, cerebrospinal fluid). (3) Application of this platform to isothermal amplification techniques, which are often difficult to design and optimize due to less established design methodologies. Being tolerant to non-specific amplification, our platform can potentially significantly accelerate the development of isothermal amplification nucleic acid tests and improve their robustness, which is of great values in emergency situations, resource-limited settings, and other scenarios.

Acknowledgements

[1]   D. A. Giljohann, C. A. Mirkin, *Nature* **2009**, *462*, 461.
[2]   P. Craw, W. Balachandran, *Lab Chip* **2012**, *12*, 2469–2486.
[3]   S. O. Kelley, C. A. Mirkin, D. R. Walt, R. F. Ismagilov, M. Toner, E. H. Sargent, *Nat. Nanotechnol.* **2014**, *9*, 969.
[4]   S. Park, Y. Zhang, S. Lin, T.-H. Wang, S. Yang, *Biotechnol. Adv.* **2011**, *29*, 830–839.
[5]   T. Notomi, H. Okayama, H. Masubuchi, T. Yonekawa, K. Watanabe, N. Amino, T. Hase, *Nucleic Acids Res.* **2000**, *28*, e63–e63.
[6]   O. Piepenburg, C. H. Williams, D. L. Stemple, N. A. Armes, *PLoS Biol.* **2006**, *4*, e204.
[7]   Q. Chou, M. Russell, D. E. Birch, J. Raymond, W. Bloch, *Nucleic Acids Res.* **1992**, *20*, 1717–1723.
[8]   E. H. Ashrafi, N. Paul, *Biotechniques* **2009**, *47*, 789–790.
[9]   A. Ruiz-Villalba, E. van Pelt-Verkuil, Q. D. Gunst, J. M. Ruijter, M. J. B. van den Hoff, *Biomol. Detect. Quantif.* **2017**, *14*, 7–18.
[10]   Y. Kimura, M. J. L. de Hoon, S. Aoki, Y. Ishizu, Y. Kawai, Y. Kogo, C. O. Daub, A. Lezhava, E. Arner, Y. Hayashizaki, *Nucleic Acids Res.* **2011**, *39*, e59–e59.
[11]   Y. Mori, T. Notomi, *J. Infect. Chemother.* **2009**, *15*, 62–69.
[12]   S. J. Reinholt, A. J. Baeumner, *Angew. Chemie Int. Ed.* **2014**, *53*, 13988–14001.
[13]   C. W. Price, D. C. Leslie, J. P. Landers, *Lab Chip* **2009**, *9*, 2484–2494.
[14]   S. C. Tan, B. C. Yiap, *Biomed Res. Int.* **2009**, *2009*.
[15]   O. Nacham, K. D. Clark, J. L. Anderson, *Anal. Chem.* **2016**, *88*, 7813–7820.
[16]   O. Nacham, K. D. Clark, M. Varona, J. L. Anderson, *Anal. Chem.* **2017**, *89*, 10661–10666.
[17]   N. Ali, R. de C. P. Rampazzo, A. D. T. Costa, M. A. Krieger, *Biomed Res. Int.* **2017**, *2017*.
[18]   B. Nasseri, N. Soleimani, N. Rabiee, A. Kalbasi, M. Karimi, M. R. Hamblin, *Biosens. Bioelectron.* **2018**, *117*, 112–128.
[19]   C. Zhang, D. Xing, *Nucleic Acids Res.* **2007**, *35*, 4223–4237.
[20]   K.-Y. Lien, W.-Y. Lin, Y.-F. Lee, C.-H. Wang, H.-Y. Lei, G.-B. Lee, *J. Microelectromechanical Syst.* **2008**, *17*, 288–301.
[21]   C.-M. Chang, W.-H. Chang, C.-H. Wang, J.-H. Wang, J. D. Mai, G.-B. Lee, *Lab Chip* **2013**, *13*, 1225–1242.
[22]   J. Yin, Y. Suo, Z. Zou, J. Sun, S. Zhang, B. Wang, Y. Xu, D. Darland, J. X. Zhao, Y. Mu, *Lab Chip* **2019**, *19*, 2769–2785.
[23]   B. H. Park, S. J. Oh, J. H. Jung, G. Choi, J. H. Seo, E. Y. Lee, T. S. Seo, *Biosens. Bioelectron.* **2017**, *91*, 334–340.
[24]   J. Wen, L. A. Legendre, J. M. Bienvenue, J. P. Landers, *Anal. Chem.* **2008**, *80*, 6472–6479.
[25]   S. H. Lee, J. Song, B. Cho, S. Hong, O. Hoxha, T. Kang, D. Kim, L. P. Lee, *Biosens. Bioelectron.* **2019**, *126*, 725–733.
[26]   C.-Y. Chao, C.-H. Wang, Y.-J. Che, C.-Y. Kao, J.-J. Wu, G.-B. Lee, *Biosens. Bioelectron.* **2016**, *78*, 281–289.
[27]   N. C. Cady, S. Stelick, C. A. Batt, *Biosens. Bioelectron.* **2003**, *19*, 59–66.
[28]   S. O. Kelley, *ACS Sensors* **2017**, *2*, 193–197.
[29]   A. Rogacs, L. A. Marshall, J. G. Santiago, *J. Chromatogr. A* **2014**, *1335*, 105–120.
[30]   L. A. Marshall, Designing Automated Systems for Sample Preparation of Nucleic Acids Using Isotachophoresis, Stanford University, **2013**.
[31]   A. Persat, L. A. Marshall, J. G. Santiago, *Anal. Chem.* **2009**, *81*, 9507–9511.
[32]   A. Persat, J. G. Santiago, *Anal. Chem.* **2011**, *83*, 2310–2316.
[33]   L. A. Marshall, A. Rogacs, C. D. Meinhart, J. G. Santiago, *J. Chromatogr. A* **2014**, *1331*, 139–142.
[34]   L. A. Marshall, C. M. Han, J. G. Santiago, *Anal. Chem.* **2011**, *83*, 9715–9718.
[35]   A. Rogacs, Y. Qu, J. G. Santiago, *Anal. Chem.* **2012**, *84*, 5858–5863.
[36]   M. Bercovici, G. V Kaigala, K. E. Mach, C. M. Han, J. C. Liao, J. G. Santiago, *Anal. Chem.* **2011**, *83*, 4110–4117.
[37]   R. B. Schoch, M. Ronaghi, J. G. Santiago, *Lab Chip* **2009**, *9*, 2145–2152.
[38]   L. A. Marshall, L. L. Wu, S. Babikian, M. Bachman, J. G. Santiago, *Anal. Chem.* **2012**, *84*, 9640–9645.
[39]   M. D. Borysiak, K. W. Kimura, J. D. Posner, *Lab Chip* **2015**, *15*, 1697–1707.
[40]   A. T. Bender, M. D. Borysiak, A. M. Levenson, L. Lillis, D. S. Boyle, J. D. Posner, *Anal. Chem.* **2018**, *90*, 7221–7229.
[41]   Y.-C. Wang, A. L. Stevens, J. Han, *Anal. Chem.* **2005**, *77*, 4293–4299.
[42]   W. Ouyang, X. Ye, Z. Li, J. Han, *Nanoscale* **2018**, *10*, 15187–15194.
[43]   D. Martins, R. Levicky, Y.-A. Song, *Biosens. Bioelectron.* **2015**, *72*, 87–94.
[44]   L. Gong, W. Ouyang, Z. Li, J. Han, *AIP Adv.* **2017**, *7*, 125020.
[45]   T. A. Zangle, A. Mani, J. G. Santiago, *Chem. Soc. Rev.* **2010**, *39*, 1014–1035.
[46]   M. Li, R. K. Anand, *Analyst* **2016**, *141*, 3496–3510.
[47]   W. Ouyang, Z. Li, J. Han, *Anal. Chem.* **2018**, *90*, 11366–11375.
[48]   N. C. Stellwagen, C. Gelfi, P. G. Righetti, *Biopolym. Orig. Res. Biomol.* **1997**, *42*, 687–703.
[49]   R. Kwak, J. Y. Kang, T. S. Kim, *Anal. Chem.* **2016**, *88*,

7

988–996.

[50] W. Ouyang, J. Han, *Proc. Natl. Acad. Sci.* **2019**, *116*, 16240–16249.

[51] B. L. Fernández-Carballo, T. Broger, R. Wyss, N. Banaei, C. M. Denkinger, *J. Clin. Microbiol.* **2019**, *57*, e01234-18.

[52] E. S. Click, W. Murithi, G. S. Ouma, K. McCarthy, M. Willby, S. Musau, H. Alexander, E. Pevzner, J. Posey, K. P. Cain, *Sci. Rep.* **2018**, *8*, 1–6.

[53] K. Murugesan, C. A. Hogan, Z. Palmer, B. Reeve, G. Theron, A. Andama, A. Somoskovi, A. Steadman, D. Madan, J. Andrews, *J. Clin. Microbiol.* **2019**, *57*, e00782-19.

[54] A. K. White, M. VanInsberghe, I. Petriv, M. Hamidi, D. Sikorski, M. A. Marra, J. Piret, S. Aparicio, C. L. Hansen, *Proc. Natl. Acad. Sci.* **2011**, *108*, 13999–14004.

[55] L. Gong, W. Ouyang, Z. Li, J. Han, *J. Memb. Sci.* **2018**, *556*, 34–41.

[56] W. Ouyang, S. H. Ko, D. Wu, A. Y. Wang, P. W. Barone, W. S. Hancock, J. Han, *Anal. Chem.* **2016**, *88*, 9669–9677.

[57] J. L. Reed, Z. J. Walker, D. Basu, V. Allen, M. P. Nicol, D. M. Kelso, S. M. McFall, *Tuberculosis* **2016**, *101*, 114–124.

[58] P. Neuzil, C. Zhang, J. Pipper, S. Oh, L. Zhuo, *Nucleic Acids Res.* **2006**, *34*, e77–e77.

[59] K. Kolari, R. Satokari, K. Kataja, J. Stenman, A. Hokkanen, *Sensors Actuators B Chem.* **2008**, *128*, 442–449.

[60] J.-H. Wang, L.-J. Chien, T.-M. Hsieh, C.-H. Luo, W.-P. Chou, P.-H. Chen, P.-J. Chen, D.-S. Lee, G.-B. Lee, *Sensors Actuators B Chem.* **2009**, *141*, 329–337.

[61] A. Cannas, D. Goletti, E. Girardi, T. Chiacchio, L. Calvo, G. Cuzzi, M. Piacentini, H. Melkonyan, S. R. Umansky, F. N. Lauria, *Int. J. Tuberc. lung Dis.* **2008**, *12*, 146–151.

8

Entry for the Table of Contents

Two-stage selective electrokinetic concentration enables one-step purification of nucleic acids and microfluidic PCR resistant to non-specific amplification, thereby significantly shortening the development cycle and simplifying the workflow of nucleic acid amplification tests for point-of-care disease diagnosis.